J. Fluid Mech. (1979), *vol.* 92, *part* 2, *pp.* 327–348
Printed in Great Britain

Autorotating flat-plate wings: the effect of the moment of inertia, geometry and Reynolds number

By J. D. IVERSEN

Department of Aerospace Engineering and Engineering Research Institute,
Iowa State University, Ames

(Received 2 November 1977)

Free-flight and wind-tunnel measurements by previous investigators of the flat-plate autorotation phenomenon have been analysed. The variation of the autorotation characteristics with changes in the Reynolds number and the aspect ratio, thickness ratio and moment of inertia of the flat plate have been correlated. The interpretation of the role of the Reynolds number made in a previous investigation is shown to be incorrect. The tip-speed ratio, for the ranges of the dimensionless parameters investigated, is shown to be a function of only the plate aspect ratio, thickness ratio, and also the moment of inertia if the latter is sufficiently small. The lift and drag coefficients, and therefore the free-flight glide angle, are shown to be functions of the tip-speed ratio, the aspect ratio and the Reynolds numbers based on the chord and plate thickness.

1. The Magnus rotor: introduction

The Magnus rotor as defined here is a cylinder of arbitrary cross-section which revolves about an axis perpendicular to the cross-section and moves through air or another fluid in a direction perpendicular to this axis (or is stationed in a wind tunnel with its axis perpendicular to the stream). Owing to the circulation about the cylinder caused by rotation and interaction with the wind stream, a lift force is generated. Some rotors, such as the circular cylinder, must be rotated by an external power source to generate circulation. Others, for example those with a flat-plate cross-section, will autorotate; that is, if once set in motion about an axis of revolution, the rotor will continue to rotate and will draw the necessary energy for doing so from the relative wind. Autorotational motion can take place either in free flight or when a plate is pinned to rotate about a given axis in a wind tunnel. A flat plate pinned to rotate about its midchord must be given an initial rotational impulse to autorotate, but there are other cross-sections, of course, which will rotate spontaneously once the wind tunnel has been started.

The concept of the Magnus rotor is not new. Gustav Magnus illustrated experimentally the existence of the lifting force on a rotating circular cylinder in 1853. In 1854, James Clerk Maxwell attempted to explain the phenomenon of an autorotating card falling through the air. His explanation was incomplete, because it does not account for the autorotation of a wind-tunnel model mounted on a bearing support.

Several applications of the Magnus rotor as lift-generating devices of both the powered and the autorotating type have been investigated. The most famous of these

0022–1120/79/4151–6490 $02.00

applications is probably the Flettner rotor ship (Ackeret 1925) of the 1920's, which employed two powered vertical circular cylinders in lieu of sails. The interest generated by the rotor ship sparked off other applications to boats and windmills. The powered circular rotor was also applied in the design of a boat propeller (Ackeret 1925). One windmill design consisted at least partially of the autorotating Savonius section (Klemin 1925; Savonius 1926; Willhoft 1927), which was also applied to small boats. The autorotating section eliminated the need for external power for the boat application. The Savonius rotor is currently used to provide the starting torque for modern wind energy devices (Blackwell 1974).

The lift and drag characteristics of powered rotors as determined by wind-tunnel testing is reported by Ackeret (1925), Reid (1924), Thom (1934), Swanson (1961) and Crabtree (1960). These tests show that the lift generated on a rotating circular cylinder is a maximum of only about half that predicted from potential theory, i.e. $L' = \rho U\Gamma$, where $\Gamma = 2\pi a^2\omega$ is the rotor circulation. More recently, transonic and supersonic tests were reported by Platou (1961). At these speeds, the Magnus force on the circular cylinder is much less than at subsonic speeds. This failure of the rotors to approach the lift predicted by potential theory caused some disappointment in the performance of the Flettner rotor ships. It also gave rise to criticism of those who espoused potential theory as an explanation of the Magnus effect (Ahlborn 1930; Regan 1966; Buford 1954). Ahlborn (1930) gives an entertaining criticism of the proponents of potential theory with a rebuttal by Hoff in the same paper. At low angles of attack of a spinning body of revolution, the Magnus force is much less than that predicted by potential theory since it does not have time to develop fully (Uselton 1966). Magnus-force prediction procedures based on analysis of the viscous boundary layer are reported by Kelly (1954), Kelly & Thacker (1956) and Power & Iversen (1973). A correlation of Magnus forces on cylinders of high fineness ratio at small angles of attack was developed by Iversen (1973). A recent interesting review of the Magnus effect on circular cylinders has been written by Jacobson (1973).

Several interesting applications of powered and autorotating rotors have been attempted for improvement of wing lift. The rotor aeroplane (Klemin 1932), in which the usual wing was replaced by powered circular cylinders, was doomed to failure from the start. Although a lift coefficient as high as 15 can be generated, a high drag coefficient of 5 results at the same time. Also, of course, power failure is immediately disastrous. The placement of a rotor somewhere in conjunction with an ordinary wing, however, can result in improvement in lift/drag characteristics. Among the earlier investigators, Reid (1924), in the United States, and Wolff & Konig (1926), in Germany, investigated the aerodynamic characteristics of airfoils with circular cylinders fitted into the leading edge. Much more recently, Alvarez-Calderon & Arnold (1961) investigated the high lift properties of wing–flap combinations with a powered circular cylinder fitted into the leading edge of the flap. The autorotating section has also been suggested for improvement of high lift characteristics (Crabtree 1960; Brunk 1965). Crabtree's configuration consists of a complete wing section with a small symmetrical rotating flap located beneath the trailing edge of the wing. The maximum lift coefficient is increased by well over a factor of 2, but the drag at maximum lift is increased by almost a factor of 5. Among many free-flight applications, the autorotating wing has been suggested as a radioactive-material containment vessel for re-entry from an earth orbit (Vorreiter & Tate 1973).

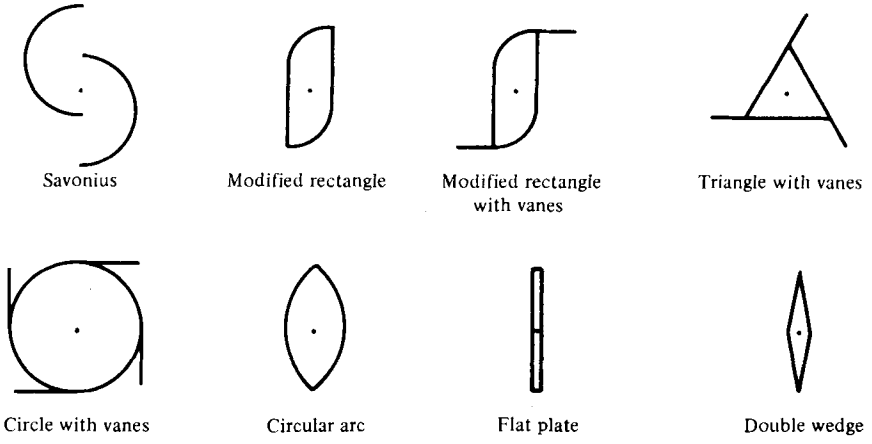

FIGURE 1. Autorotor cross-sections.

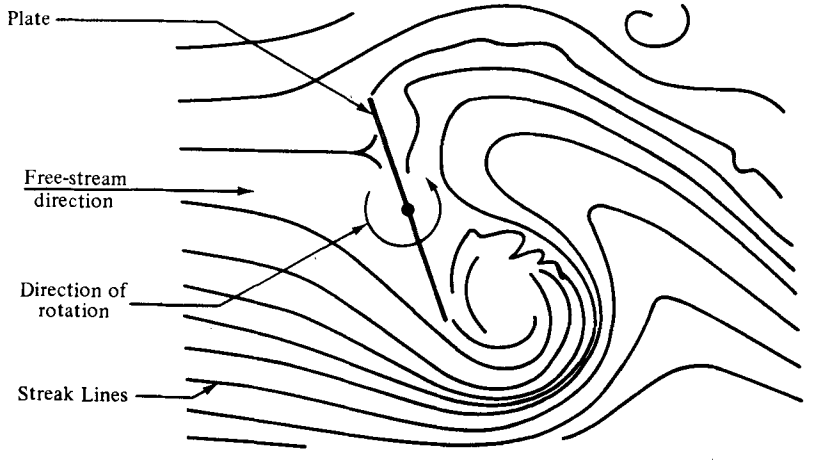

FIGURE 2. Sketch from smoke-tunnel photograph of an autorotating flat plate (from Yelmgren 1966). Note large vortex downstream of the retreating edge.

In this paper, the autorotation phenomenon of the flat-plate wing is analysed by considering free-flight and wind-tunnel data gathered by previous investigators. The data are analysed by correlating the tip-speed ratio and lift and drag coefficients with functions of the aspect ratio, thickness ratio, moment-of-inertia parameter and thickness and chord Reynolds numbers.

2. Theory of wing autorotation

Various types of autorotating cross-sections are shown in figure 1. It may be fairly obvious why the five asymmetric sections autorotate, at least those with driving vanes. (Experiments by various investigators on autorotors of asymmetric section are reported in Iversen 1969.) The three symmetric sections, the circular arc, flat plate and double wedge, however, require closer examination. As mentioned previously, Maxwell (1854) was the first to try to explain the flat-plate autorotation phenomenon. He hypothesized that the autorotation was caused by a decrease in lift force due to continuing deceleration of the rotor as it descends through the air. His explanation,

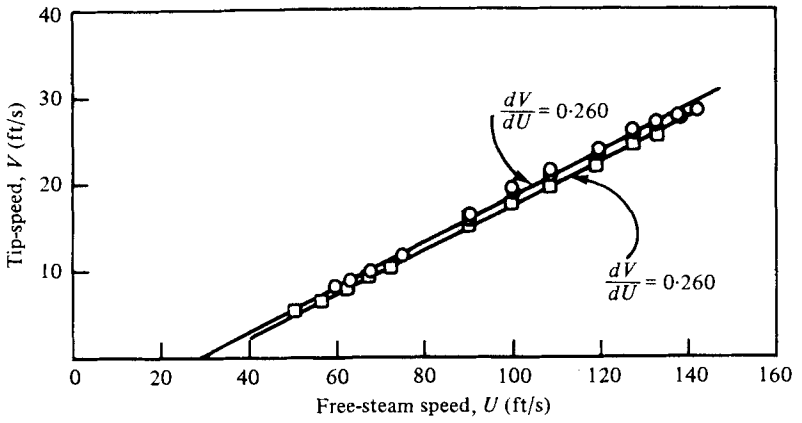

FIGURE 3. Rotor tip-speed *vs.* free-stream speed; effect of bearing friction. Wind-tunnel data from Glaser & Northup; aspect ratio = 0·5, thickness ratio = 0·0313. ○, normal bearing friction; □, high bearing friction.

seemingly valid for the falling rotor, does not explain autorotation in a wind tunnel and so is incomplete even for the falling rotor.

Riabouchinsky (1935) based his explanation on a hypothesized change in the shape of the wake as the rotor revolves. He assumed that the wake is small when the retreating side of the rotor is at an angle of less than $\frac{1}{2}\pi$ to the free stream, and that the wake is large when the advancing side is at an angle of less than $\frac{1}{2}\pi$ to the free stream. Thus the lift generated is larger in the former case, and the average moment about the axis of rotation would be in the direction of rotation.

Bustamante & Stone (1969), Iversen (1969) and Smith (1970, 1971) have suggested that autorotation of wings of symmetrical cross-section is due to a large vortex shed from the retreating face of the wing cross-section. It has been shown theoretically (Iversen 1969) that such a vortex creates an aerodynamic moment tending to continue autorotation. A smoke-tunnel photograph of streak lines taken by Yelmgren (1966) is sketched in figure 2. A large vortex shed from the retreating (downstream) face of the rotor is shown, while no similar vortex is visible from the advancing face.

3. Tip-speed ratio: effect of bearing friction

Typical examples of the tip speed V as a function of the free-stream test-section speed U for a flat-plate rotor are plotted in figure 3. The friction of the bearings obviously affects these data as the straight lines plotted through the data do not pass through the origin. The effect of the bearing friction can be found in the following approximate manner. It is assumed that the average aerodynamic moment about the centre of rotation in the direction of rotation is

$$M_A = k_1 U^2 - \tfrac{1}{2} k_2 U \dot{\theta} c, \tag{1}$$

where c is the wing chord and θ the rotor angle of attack. The first term is a driving moment and the second represents aerodynamic damping. The dot indicates the derivative with respect to time. The bearing friction is assumed to be

$$M_B = -k_3 \exp(-k_4 \dot{\theta}) - k_5 \dot{\theta} - k_6 U. \tag{2}$$

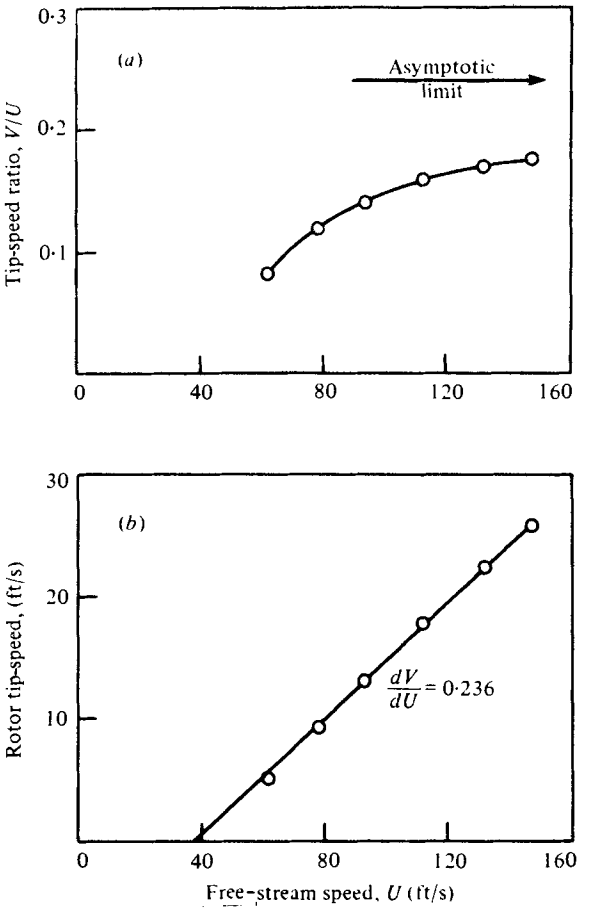

FIGURE 4. (*a*) Rotor tip-speed ratio and (*b*) tip-speed *vs.* free-stream speed. Plotting V/U (or the Strouhal number) *vs.* U (or the Reynolds number) does not enable one to calculate the large U tip-speed ratio as does plotting V *vs.* U. Wind-tunnel data, double wedge, aspect ratio = 0·5, aluminium rotor.

The first term provides the static retarding torque, the second is the retarding torque due to rotation and the third increases with speed owing to the increased force on the bearing. The k's are all positive constants. Thus the equation of motion is

$$k_1 U^2 - \tfrac{1}{2}k_2 U\dot{\theta}c - k_3 \exp(-k_4\dot{\theta}) - k_5\dot{\theta} - k_6 U = I\ddot{\theta}, \tag{3}$$

where I is the moment of inertia of the rotor. At equilibrium rotor speed ($\ddot{\theta} = 0$)

$$\dot{\theta} = \frac{k_1 U^2 - k_3 \exp(-k_4\dot{\theta}) - k_6 U}{\tfrac{1}{2}k_2 Uc + k_5}. \tag{4}$$

At large values of U and therefore $\dot{\theta}$, (4) can be approximated by

$$\dot{\theta} \cong \frac{2k_1}{k_2 c}U - \frac{2k_6}{k}, \quad \text{or} \quad \frac{V}{U} = \frac{c\dot{\theta}}{2U} = \frac{k_1}{k_2} - \frac{k_6}{k_2 U}, \quad V = \frac{k_1}{k_2}U - \frac{k_6}{k_2}. \tag{5}$$

Thus the effect of bearing friction can be largely ignored, provided that k_3 and k_5 are small enough, by taking for the value of V/U the slope of the experimental curve at a higher value of the velocity.

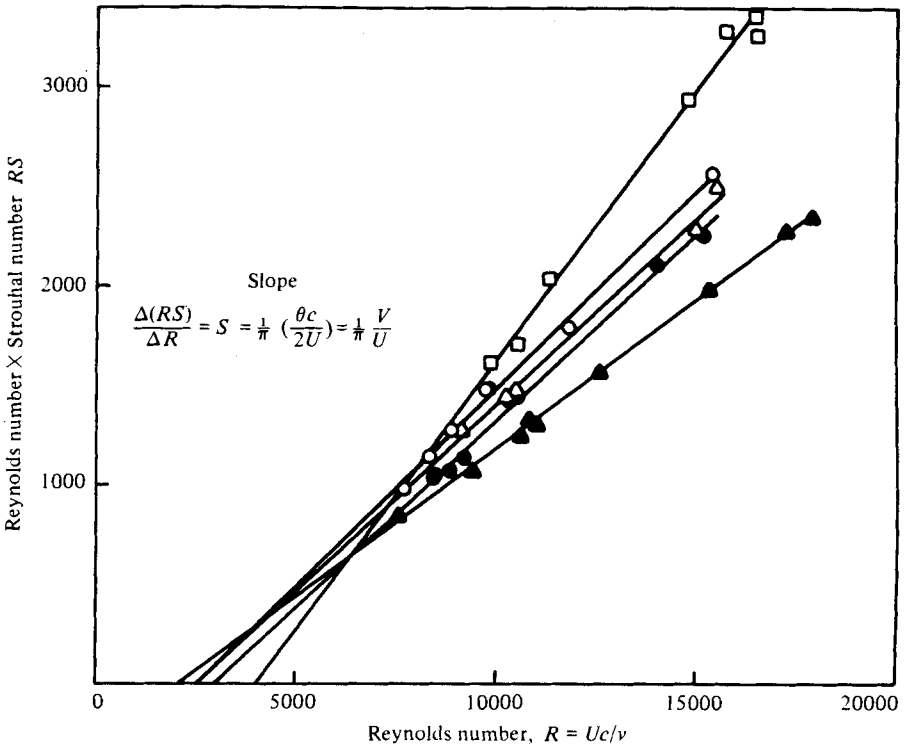

FIGURE 5. Wind-tunnel data from Smith (1970) replotted in order to obtain curve slopes (V/U for large U). ▲, $S = 0{\cdot}147$, $V/U = 0{\cdot}461$; ●, $S = 0{\cdot}188$, $V/U = 0{\cdot}590$; △, $S = 0{\cdot}188$, $V/U = 0{\cdot}590$; ○, $S = 0{\cdot}200$, $V/U = 0{\cdot}628$; □, $S = 0{\cdot}273$, $V/U = 0{\cdot}857$.

The effect of bearing friction has been misinterpreted by Smith (1970, 1971). He assumed that the tip-speed ratio V/U (or Strouhal number $V/\pi U$) measured experimentally in a wind tunnel is a function of the Reynolds number, and presented data in which the tip-speed ratio gradually increases with increasing Reynolds number. This increase in the tip-speed ratio (or Strouhal number), however, is due to bearing friction, not the Reynolds number. Figure 4(*a*) reproduces data (Iversen 1969) for the tip-speed ratio V/U *vs.* the free-stream speed U for a 0·5 aspect ratio rotor. A curve of Strouhal number *vs.* Reynolds number (as in Smith 1970, 1971) could be obtained by changing the vertical scale by a factor of $1/\pi$ and the horizontal scale by a factor of c/ν, where ν is the kinematic viscosity. The resulting curve shape strongly resembles Smith's data. In figure 4(*b*) the same data for the tip speed V are plotted *vs.* the free-stream speed U. The slope of the curve, as predicted by (5), is the expected free-flight autorotation value of V/U, which would be reached only in the limit of much larger U in figure 4(*a*). Similarly, if Smith's data are replotted, straight lines are also obtained in plots of V *vs.* U. The tip-speed ratio V/U is thus calculated as a single value instead of as a function of the Reynolds number. Five of his experiments are replotted in figure 5 (from figure 31, Smith 1970). The values of V/U calculated from the slopes in figure 5 range from 0·46 to 0·86. In contrast, the maximum values of V/U that he measured range from 0·42 to 0·66, the latter figure being 23 % less than the projected free-flight value of 0·86. The variation in tip-speed ratio with Reynolds number for his

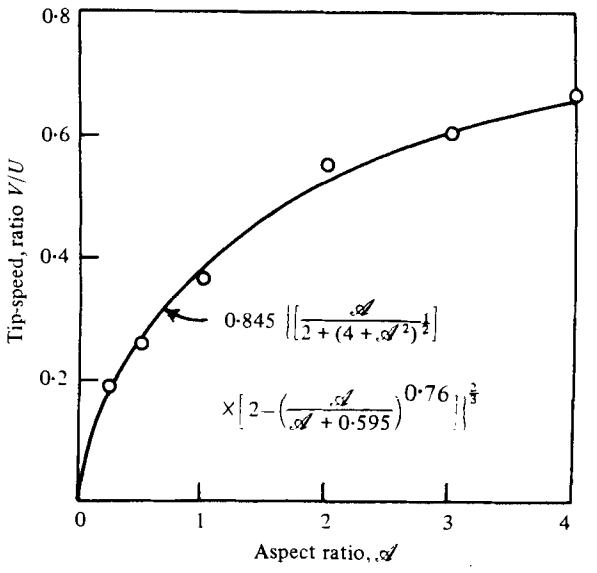

FIGURE 6. Tip-speed ratio *vs.* aspect ratio. Wind-tunnel data from Glaser & Northup, $\tau = 0{\cdot}03125$, $6{\cdot}1 \leqslant K \leqslant 6{\cdot}5$.

range of Reynolds numbers should be small because the autorotating-wing phenomenon is largely involved with time-dependent sharp-edged separation. Any functional relationship with the Reynolds number is likely to be masked by the effects of bearing friction.

4. Tip-speed ratio: effect of aspect ratio

Glaser & Northup (1971) carried out a systematic series of wind-tunnel tests to determine the tip-speed ratio of flat-plate autorotors for various aspect ratios, moments of inertia and thickness ratios. Figure 6 shows their data for tip-speed ratio *vs.* aspect ratio for a constant thickness ratio $\tau = t/c$ (where t is the plate thickness) and a nearly constant value of the moment-of-inertia parameter $K = I/\rho c^4 b$.

Also shown in figure 6 is the curve of an equation derived as follows. The static stability derivative $C_{m\alpha}$ about the half-chord line of an unswept wing can be written as

$$C_{m\alpha} = C_{L\alpha} \quad (0{\cdot}5 - h_n), \tag{6}$$

where $C_{L\alpha}$ is the lift-curve slope and h_n is the distance of the aerodynamic centre from the leading edge divided by the chord. A good empirical expression for $C_{L\alpha}$ for rectangular wings was given by Diederich (1951) as

$$C_{L\alpha} = a_0 \mathscr{A}/\{a_0/\pi + \mathscr{A}[1 + (a_0/\pi\mathscr{A})^2]^{\frac{1}{2}}\}, \tag{7}$$

where $\mathscr{A} = b/c$ is the aspect ratio. With the two-dimensional lift-curve slope a_0 set equal to the thin-airfoil value of 2π, (7) becomes

$$C_{L\alpha}/2\pi = \mathscr{A}/[2 + (4 + \mathscr{A}^2)^{\frac{1}{2}}]. \tag{8}$$

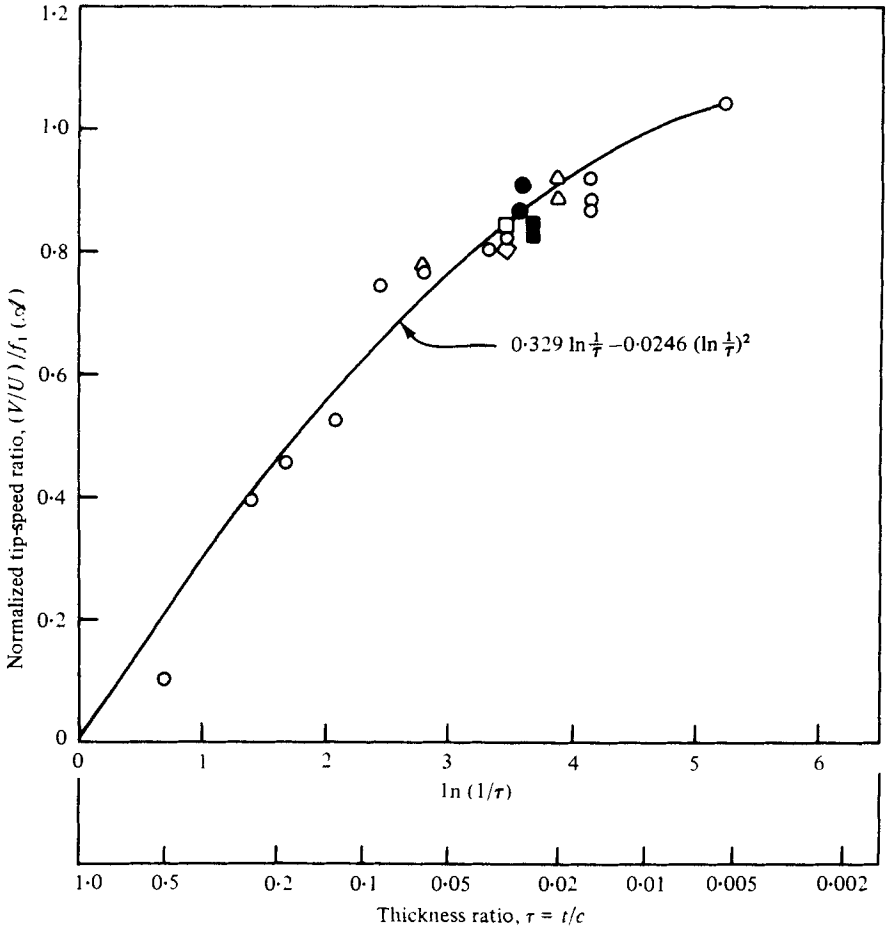

FIGURE 7. Normalized tip-speed ratio *vs.* thickness ratio.

		$\mathscr{A}$	K		$\mathscr{A}$	K
Wind-tunnel data, Glaser & Northup	⊖	0·25	6·5	△	2	4·1–13·8
	○	0·5	1·3–32	□	3	6·1
	◇	1	6·2	⊟	4	6·1
Free-flight data, Bustamente & Stone	■	1·185	3·9	●	2·667	6·7

An empirical expression for h_n for rectangular wings was fitted to data from a variety of sources:

$$h_n = 0{\cdot}25[\mathscr{A}/(\mathscr{A} + 0{\cdot}595)]^{0{\cdot}76}. \tag{9}$$

Thus the resulting expression for $C_{m\alpha}$ (about the half-chord line) for rectangular wings at small angles of attack is

$$2C_{m\alpha}/\pi = [\mathscr{A}/\{2 + [4 + (\mathscr{A})^2]^{\frac{1}{2}}\}]\{2 - [\mathscr{A}/(\mathscr{A} + 0{\cdot}595)]^{0{\cdot}76}\}. \tag{10}$$

On the premise that the aerodynamic overturning moment for small angles of attack might be a valid correlation parameter for the autorotating plate as well, (10) was

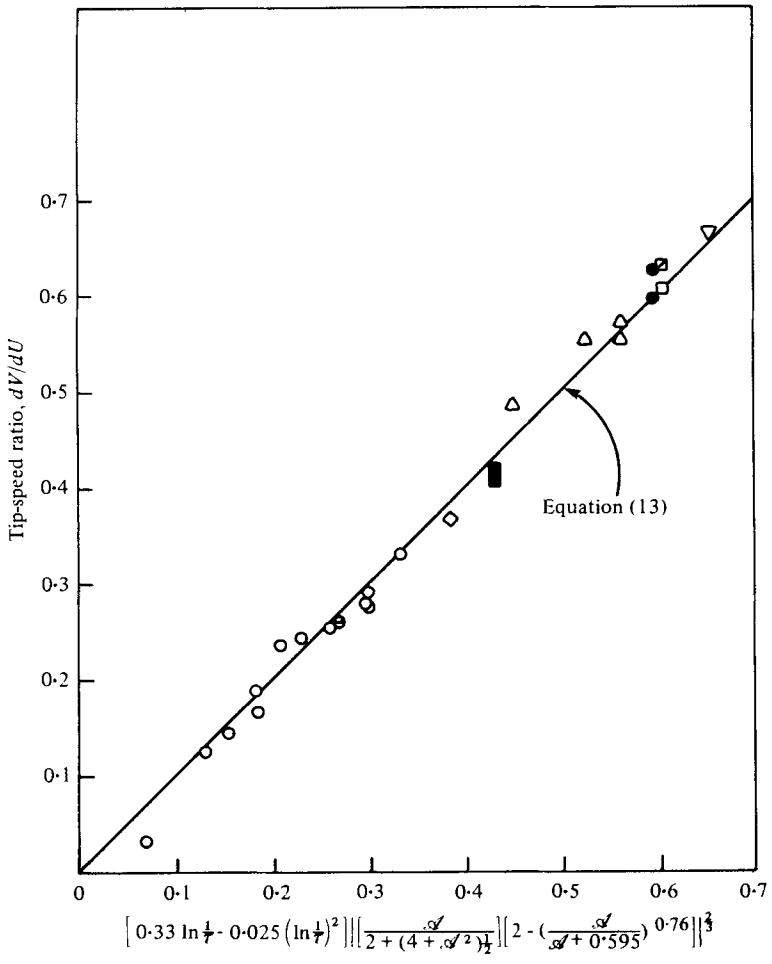

FIGURE 8. Tip-speed ratio *vs.* thickness-ratio–aspect ratio function.

		$\mathscr{A}$	τ	K
Wind-tunnel data, Glaser & Northup	⊖	0·25	0·0313	6·48
	○	0·5	0·0054–0·50	1·31–32·1
	◇	1	0·0313	6·18
	△	2	0·0208–0·0625	4·06–11·31
	□	3	0·0313	6·11
	⊟	3·048	0·0318	16·90
	▽	4	0·0313	6·10
Free-flight data, Bustamente & Stone	■	1·185	0·0256	3·93
	●	2·667	0·0278	6·68

applied to the data shown in figure 6. An excellent fit is obtained by letting the tip-speed ratio be proportional to the parameter in (10) to the two-thirds power. Thus

$$V/U = f_2(\tau)f_3(I/\rho c^4 b)\left\{\left[\frac{\mathscr{A}}{2+(4+\mathscr{A}^2)^{\frac{1}{2}}}\right]\left[2-\left(\frac{\mathscr{A}}{\mathscr{A}+0{\cdot}595}\right)^{0{\cdot}76}\right]\right\}^{\frac{2}{3}}$$
$$= f_1(\mathscr{A})f_2(\tau)f_3(I/\rho c^4 b). \tag{11}$$

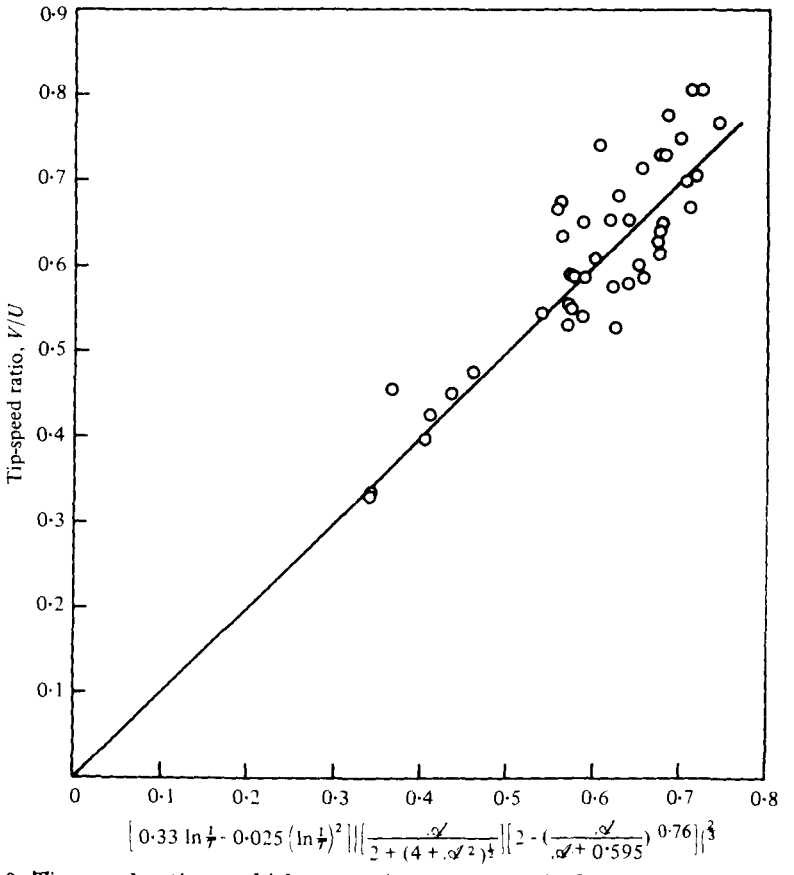

FIGURE 9. Tip-speed ratio *vs.* thickness ratio – aspect ratio function. Free-flight data from Dupleich; $0{\cdot}8 < \mathscr{A} < 6$, $0{\cdot}0074 < \tau < 0{\cdot}167$, $0{\cdot}028 < K < 0{\cdot}62$.

5. Tip-speed ratio: effect of thickness ratio

A second series of experiments was undertaken by Glaser & Northup (1971) to determine the effect of the thickness ratio $\tau = t/c$ on the tip-speed ratio V/U. Thickness ratios τ ranging from 0·0054 to 0·5 were tested. The effect of the aspect ratio can be eliminated by plotting the ratio $(V/U)/f_1(\mathscr{A})$ [as defined in (11)] *vs.* thickness ratio τ as in figure 7. The effect of a change in the moment-of-inertia parameter K $(= I/\rho c^4 b)$ is very small for values of K greater than one, so only data for these values of K are plotted (see Smith 1970 and below). Free-flight data from Bustamante & Stone (1969) for much higher Reynolds numbers are also shown in figure 7. A fairly good fit to the data is obtained with

$$f_2(\tau) = 0{\cdot}329 \ln \tau^{-1} - 0{\cdot}0246 (\ln \tau^{-1})^2. \tag{12}$$

Normalizing V/U by $f_1(\mathscr{A})$ has the effect of emphasizing data scatter, so the data are replotted in figure 8 according to

$$V/U = f_1(\mathscr{A}) f_2(\tau) = (0{\cdot}329 \ln \tau^{-1} - 0{\cdot}0246 \ln \tau^{-1})^2 \left\{\left[\frac{\mathscr{A}}{2+(4+\mathscr{A}^2)^{\frac{1}{2}}}\right]\left[2-\left(\frac{\mathscr{A}}{\mathscr{A}+0{\cdot}595}\right)^{0{\cdot}76}\right]\right\}^{\frac{3}{2}}. \tag{13}$$

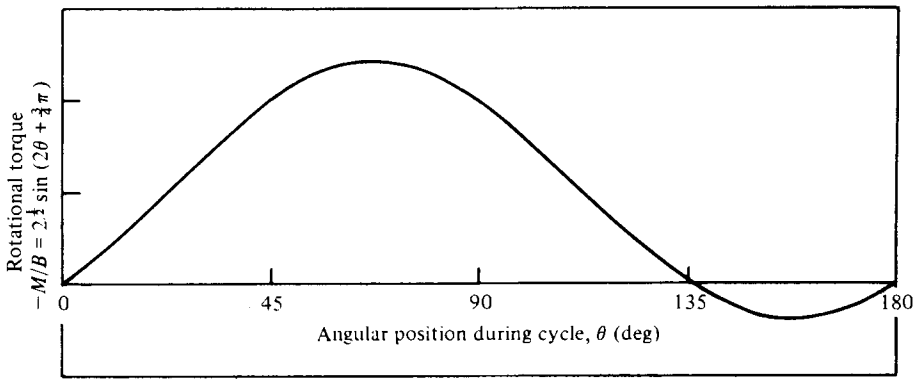

FIGURE 10. Stylized rotational torque as a function of cyclic angle θ used in numerical solution.

In this case the data scatter appears to be small considering the ranges of the aspect ratio (0·25–4) and thickness ratio (0·0054–0·5) covered. Equation (13) should thus give fairly good predictions of the free-flight tip-speed ratio for $K > 1$. A similar plot is shown for Dupleich's (1941) data in figure 9, also for a large range of aspect ratios and thickness ratios. There is more scatter in these data, which are all for free flight, than in figure 8, but as shown later, this is due to the small values (< 1) of the inertia parameter K. Equation (13) still fits the data fairly well, however.

6. Tip-speed ratio: effect of moment of inertia

The equation of motion for a flat-plate autorotor with one degree of freedom (mounted in a wind tunnel) and linear damping is

$$I\ddot{\theta} + D_0\dot{\theta} + M_A(\theta) = 0, \tag{14}$$

where $D_0\dot{\theta}$ is the rotor damping torque. A stylized aerodynamic moment $M_A(\theta)$ which is not unlike Smith's experimental lift curves (Smith 1970, figure 12, or 1971, figure 6)† was devised for the purpose of illustrating the effect of the moment of inertia:

$$M_A(\theta) = B[2\tfrac{1}{2}\sin(2\theta + \tfrac{3}{4}\pi) - 1]. \tag{15}$$

This equation is shown for one half-cycle in figure 10. It provides a net average moment during the cycle tending to continue autorotation. The damping factor D_0 is assumed to be constant and would, of course, include the effect of bearing friction for wind-tunnel data. Incorporating (15) into a dimensionless version of (14) results in

$$d^2\theta + \frac{C_U}{K}d\theta + 2\tfrac{1}{2}\frac{C_B}{K}\sin(2\theta + \tfrac{3}{4}\pi) = \frac{C_B}{K}, \tag{16}$$

where

$$d = (c/2U)\,d/dt, \quad C_B = B/\tfrac{1}{2}\rho U^2 bc^2, \quad C_U = D_0/\tfrac{1}{4}\rho U b c^3, \quad K = I/\rho c^4 b. \tag{17}$$

Equation (16) was first solved numerically with $C_B = 1$, $C_U = 1$ and initial values of θ and $d\theta$ of 0·1 and 0 for values of K from 1 to 100. The ratio C_B/C_U is the steady-state tip-speed ratio V/U for large K. After a period of time, the numerical solutions

† It appears that the top and bottom ordinate legends should be interchanged on figure 6 of Smith (1971).

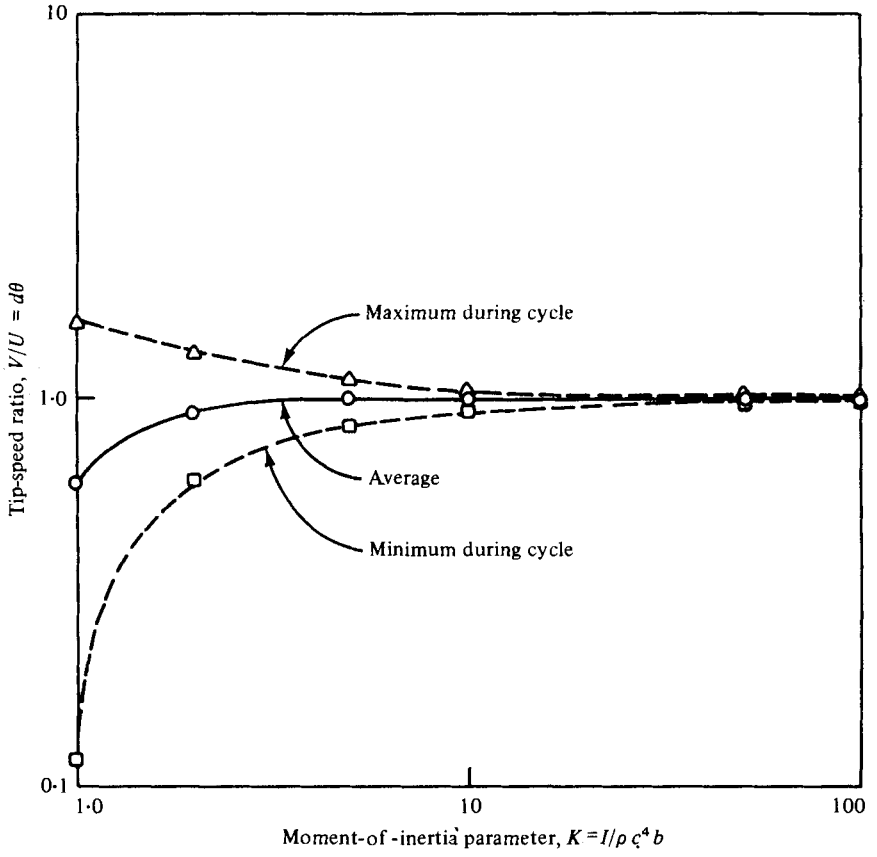

FIGURE 11. Tip-speed ratio *vs.* moment of inertia parameter: numerical solution of $d^2\theta + (C_U/K)\, d\theta + 2(C_B/K) \sin(2\theta + \frac{3}{4}\pi) = C_B/K$, $C_B = 1$, $C_U = 1$.

approached a steady state (i.e. identical half-cycles). The resulting steady-state minimum, average and maximum speed ratios during the cycle are shown in figure 11. Obviously, for low values of K the tip-speed ratio varies greatly during the cycle. As K is decreased, a point is reached where the inertia of the rotor is not great enough to carry it through the retarding-moment portion of the cycle, and autorotation cannot be maintained.

Experimental values of the minimum K for autorotation (K_M) and curves similar to the average curve of figure 11 were obtained by Glaser & Northup (1971) and Smith (1970) and are illustrated in figure 12. The values of K_M of somewhat less than 0·2 (Glaser & Northup) and 0·06 (Smith) are, of course, dependent upon bearing friction. Smith's bearing friction is smaller, so he was able to obtain lower values of K_M.

Equation (16) was again solved numerically, the values of C_B and C_U being continually adjusted in order to obtain a finite-difference solution which matched the $\mathscr{A} = 5$ data in figure 12. The results are shown in figure 13. The closeness of fit is reasonably good for the wind-tunnel case. The effect of variation of the moment of inertia, then, at least for the wind-tunnel results, is extremely rapid at and just above K_M. However, the tip-speed ratio is within 80 % of the large-K asymptotic limit for the experimental data for a value of $K/K_M = 1{\cdot}15$ and within 90 % for $K/K_M = 1{\cdot}8$.

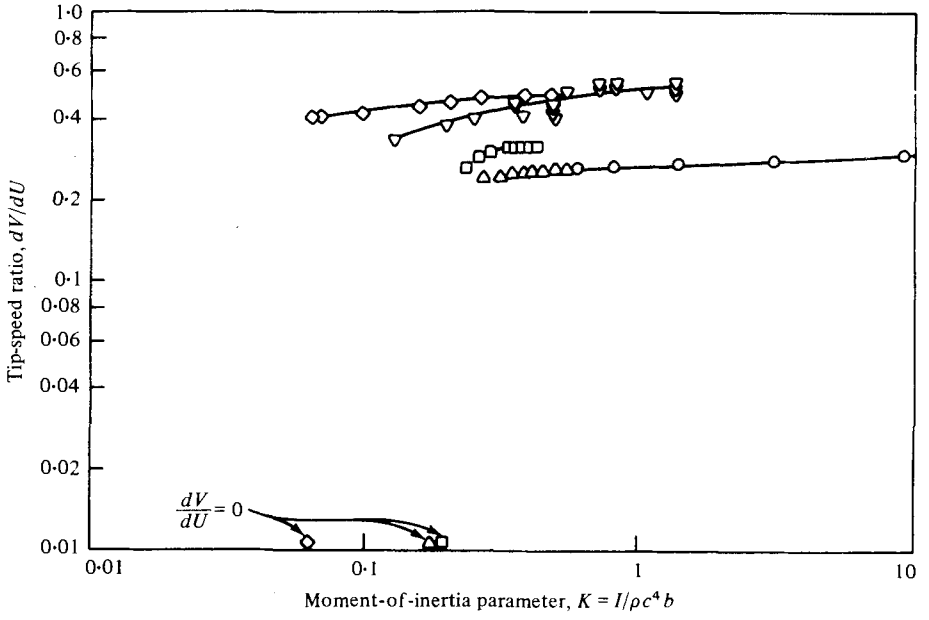

FIGURE 12. Tip-speed ratio *vs.* moment-of-inertia parameter: experimental (wind-tunnel) data. Glaser & Northup: ○, $\mathscr{A} = 0{\cdot}5$, $\tau = 0{\cdot}01563$, aluminium plate; △, $\mathscr{A} = 0{\cdot}5$, $\tau = 0{\cdot}1563$, balsa plate; □, $\mathscr{A} = 1{\cdot}0$, $\tau = 0{\cdot}1563$, balsa plate. Smith: ▽, $\mathscr{A} = 6{\cdot}4$, tip plates, flat plate; ◇, $\mathscr{A} = 3{\cdot}0$, tip plates, ellipse.

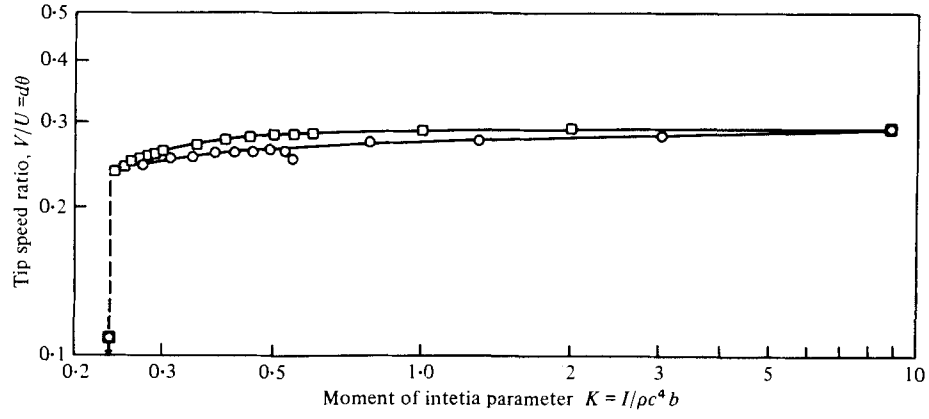

FIGURE 13. Tip-speed ratio *vs.* moment-of-inertia parameter: comparison of numerical solution and experiment. ○, wind-tunnel data from Glaser & Northup, $\mathscr{A} = 0{\cdot}5$, $t/c = 0{\cdot}0156$; □, numerical solution of $d^2\theta + (C_U/K)\,d\theta + 2\frac{1}{2}(C_B/K)\sin(2\theta + \frac{3}{4}\pi) = C_B/K$, $C_B = 0{\cdot}03100$, $C_U = 0{\cdot}07216$.

For practical purposes, the tip-speed ratio nears the large-K limit for comparatively small values of K (> 1).

To compare the effect of moment of inertia for free-flight and wind-tunnel data, figure 14 was prepared. This figure illustrates the tip-speed ratio V/U normalized by the thickness and aspect-ratio parameters, i.e.

$$(V/U)/[f_1(\mathscr{A})f_2(\tau)] = f_3(K). \tag{18}$$

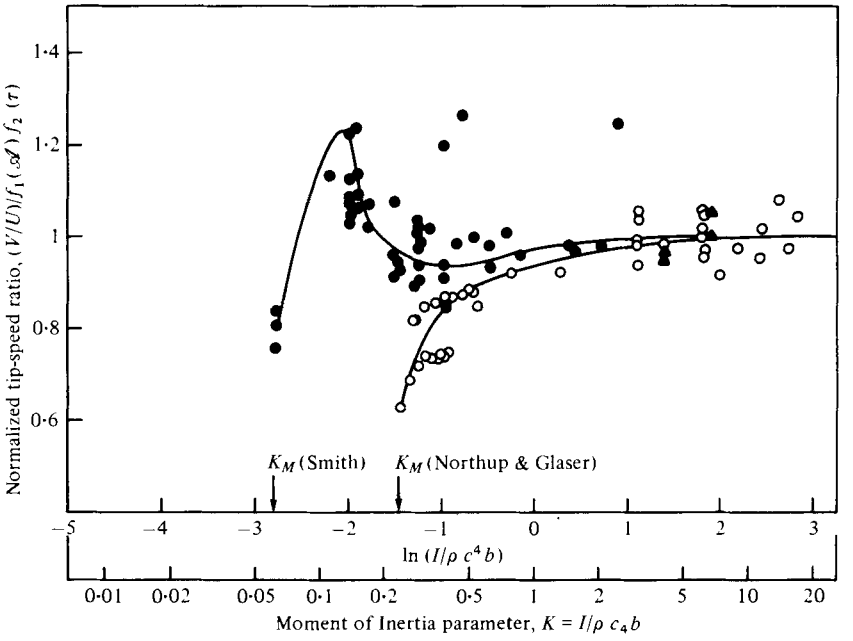

FIGURE 14. Normalized tip-speed ratio *vs.* moment-of-inertia parameter. Free-flight and wind-tunnel data. ●, free flight, Dupleich, $\mathscr{A} = 0{\cdot}8$–6, $t/c = 0{\cdot}003$–$0{\cdot}167$; ▲, free flight, Bustamente & Stone, $\mathscr{A} = 1{\cdot}19$, $2{\cdot}67$, $t/c = 0{\cdot}026$, $0{\cdot}028$; ○, wind tunnel, Glaser & Northup, $\mathscr{A} = 0{\cdot}25$–4, $t/c = 0{\cdot}005$–$0{\cdot}25$.

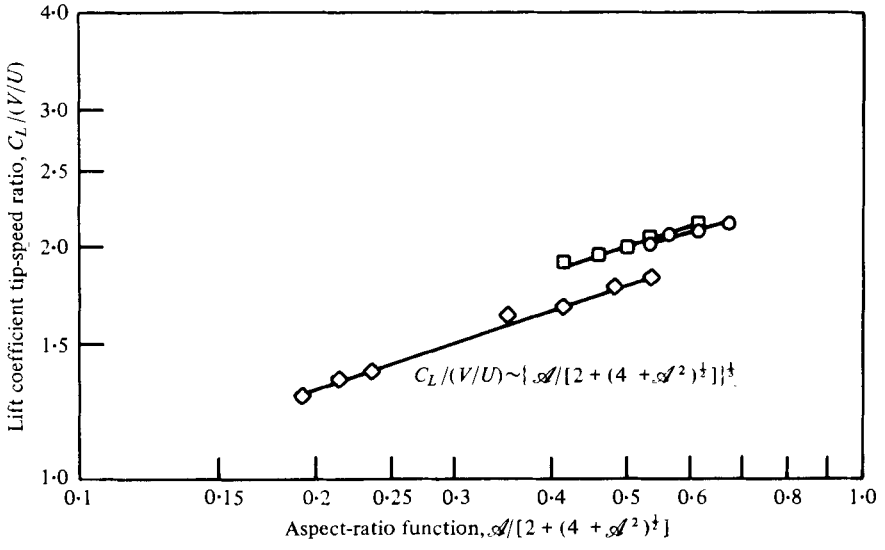

FIGURE 15. Lift coefficient tip-speed ratio *vs.* aspect-ratio function. Free-flight data from Dupleich. □, $Ut/\nu = 38$–50, $t/c = 0{\cdot}020$; ○, $Ut/\nu = 42$–47, $t/c = 0{\cdot}010$; ◇, $Ut/\nu = 86$–$1{\cdot}04$, $t/c = 0{\cdot}009$.

Again, this method of plotting emphasizes data scatter, but the difference between the wind-tunnel and free-flight cases (i.e. the effect of bearing friction) is still well illustrated. First of all, in Dupleich's (1941) free-flight data there appears to be an overshoot in the tip-speed ratio for values of K from 0·08 to 0·2 which is not observed in either the wind-tunnel data or the numerical solution of (16). Second, the minimum K for autorotation (K_M) is significantly lower ($K_M < 0{\cdot}06$; Dupleich discussed the existence of a minimum K but did not give a value). Third, Smith's value of K_M (0·06) is significantly lower than Glaser & Northup's (0·24) because of lower bearing friction but is still apparently higher than Dupleich's free-flight value. Fourth, in the limit of large moment of inertia the normalized tip-speed ratio is the same (within the data scatter) for the wind-tunnel as it is for the free-flight case, verifying the use of the slope of the V *vs.* U curves as the correct value of the tip-speed ratio. Thus, for large moment of inertia, (13) can be used to predict tip-speed ratios in free flight for flat-plate autorotating wings. Obviously, a different aerodynamic forcing moment function would be needed in (16) in order to reproduce Dupleich's data for small K. A normalized tip-speed ratio involving the thickness and aspect ratios may not be sufficiently complicated for small moment of inertia; this may account for some of the data scatter. Analysis of Dupleich's data seems to show no effect of the Reynolds number on the tip-speed ratio, although the lift and drag coefficients are affected as shown below.

7. Flat-plate autorotation: lift and drag

Lift and drag coefficients can be calculated from Dupleich's free-flight data since the flight-path glide angle and speed and the plate weights were recorded. The resulting lift coefficients for three thickness ratios are shown in figure 15. It should be noted that the lift and drag coefficients calculated were based on the standard sea-level air density since Dupleich did not list air-density information. The resulting coefficients are thus probably slightly low. The lift on a rotating wing can be expressed as

$$L = \rho U \Gamma b, \tag{19}$$

where Γ is an average value of the circulation along the span. The circulation Γ should be proportional to product of the tip speed and the chord:

$$\Gamma = K\pi V c, \tag{20}$$

where the coefficient K is probably a strong function of the aspect ratio. Thus the lift coefficient is

$$C_L = 2\pi(V/U) f(\mathscr{A}). \tag{21}$$

The ratio $C_L(V/U)^{-1}$ is plotted as a function of $\mathscr{A}$ [from (8) for the lift-curve slope] in figure 15 and turns out to be proportional to the lift-curve slope aspect ratio function to the one-third power. It appears from this figure that the coefficient of proportionality is a function of the thickness Reynolds number Ut/ν. (Other functional relationships were attempted but did not work.) Thus the ratio

$$C_L[(V/U)\{\mathscr{A}/[2+(4+\mathscr{A}^2)^{\frac{1}{2}}]\}^{\frac{1}{2}}]^{-1}$$

is plotted in figure 16, where the correlation is seen to be remarkably good. To illustrate the degree of correlation, the lift coefficient is plotted *vs.* the adjusted tip-speed ratio in figure 17:

$$C_L = (V/U)\{\mathscr{A}/[2+(4+\mathscr{A}^2)^{\frac{1}{2}}]\}^{\frac{1}{3}} f_4(Ut/\nu), \tag{22}$$

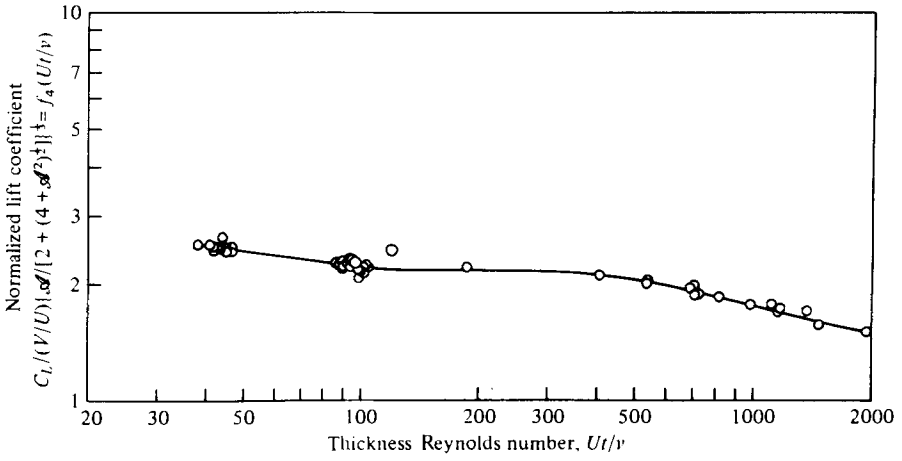

FIGURE 16. Normalized lift coefficient *vs.* thickness Reynolds number. Free-flight data, from Dupleich, $0{\cdot}8 \leqslant \mathscr{A} \leqslant 6$, $0{\cdot}0074 \leqslant \tau \leqslant 0{\cdot}167$.

where the function $f_4(Ut/\nu)$ is the ordinate of the solid line in figure 16. The correlation is remarkably good, illustrating the care with which Dupleich performed his experiments. The lift coefficient is not sensibly a function of the chordwise Reynolds number, but is a function of the thickness Reynolds number, indicating that the circulation is affected by the plate thickness in such a way that the lift decreases with an increase in thickness. There appear to be two distinct Reynolds number regimes in figure 16, one for Reynolds numbers less than 100 and another for Reynolds numbers greater than 500, in which the lift decreases with increasing Reynolds number. From 100 to 500, the normalized lift coefficient is nearly constant. Some kind of transition is apparently taking place. The drag coefficient, as shown below, is a function of both the chordwise and the thickness Reynolds number, and a more distinct transition occurs in the same thickness Reynolds number regions.

As has been demonstrated before (Iversen 1969), the drag coefficient C_D is independent of the aspect ratio and therefore of the tip-speed ratio, as illustrated by Dupleich's data for three thickness ratios shown in figure 18. It is, however, a function of the chord Reynolds number as shown in figure 19. Three separate curves appear when the drag-coefficient data are plotted as a function of the chord Reynolds number, corresponding to different values of the thickness Reynolds number. For a constant thickness Reynolds number, the drag coefficient increases with chord Reynolds number, but the increase is not as large for larger thickness Reynolds numbers. For average thickness Reynolds numbers of 44 (38–47) and 95 (91–104), C_D is proportional to $(Uc/\nu)^{0{\cdot}225}$, but for an average thickness Reynolds number of 711 (693–725), C_D is proportional to $(Uc/\nu)^{0{\cdot}12}$.

The ratios $C_D(Uc/\nu)^{-0{\cdot}225}$ for $38 \leqslant Ut/\nu \leqslant 104$ and $C_D(Uc/\nu)^{-0{\cdot}12}$ for

$$119 \leqslant Ut/\nu \leqslant 1930$$

are shown in figure 20. Clearly, the drag coefficient decreases with an increase in thickness Reynolds number, a very interesting result. Again, the variation with Reynolds number is more rapid for the lower Reynolds numbers and, as for the lift coefficient, there must be a significant change in the flow characteristics as the thickness Reynolds number is increased through 100.

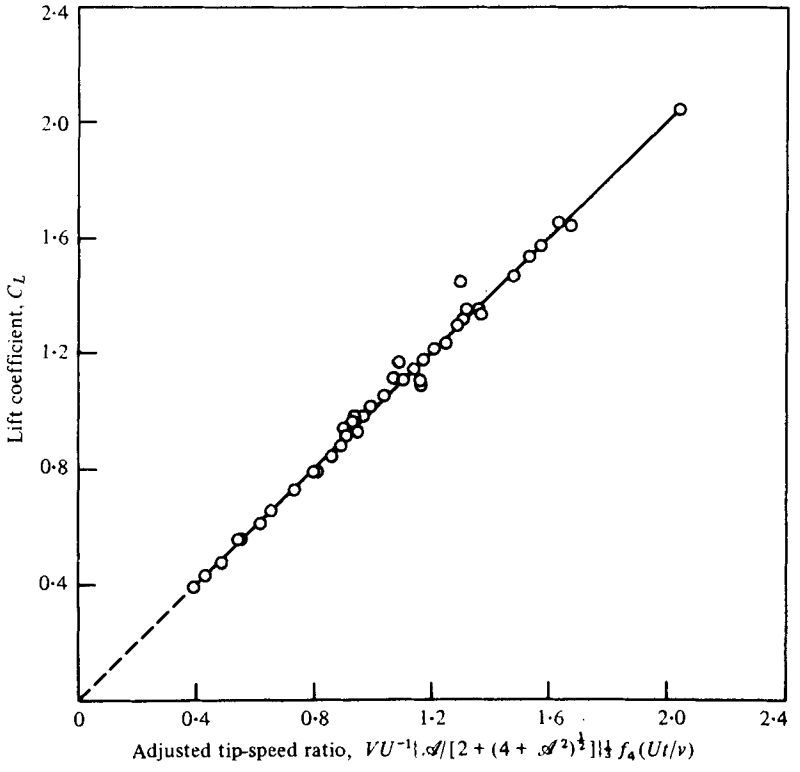

FIGURE 17. Lift coefficient *vs.* adjusted tip-speed ratio. Free-flight data from Dupleich, $0{\cdot}8 \leqslant \mathscr{A} \leqslant 6$, $0{\cdot}0074 \leqslant \tau \leqslant 0{\cdot}67$, $38 \leqslant Ut/\nu \leqslant 1930$.

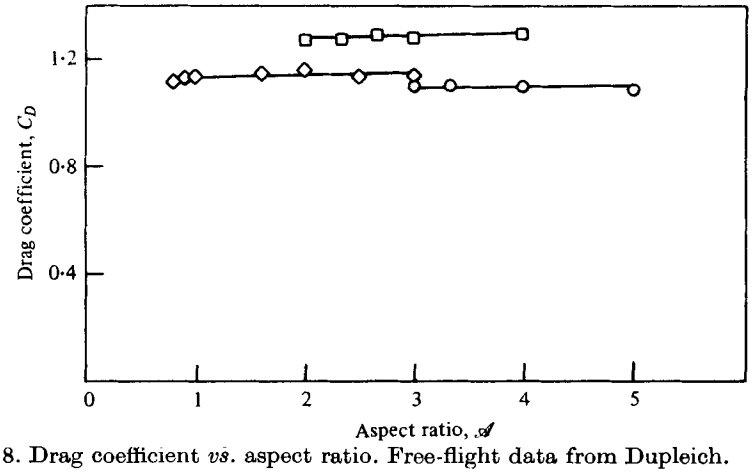

FIGURE 18. Drag coefficient *vs.* aspect ratio. Free-flight data from Dupleich.

	Ut/ν	t/c	Uc/ν
□	38–45	0·020	3880–4540
○	42–47	0·010	2150–2380
◇	86–104	0·009	

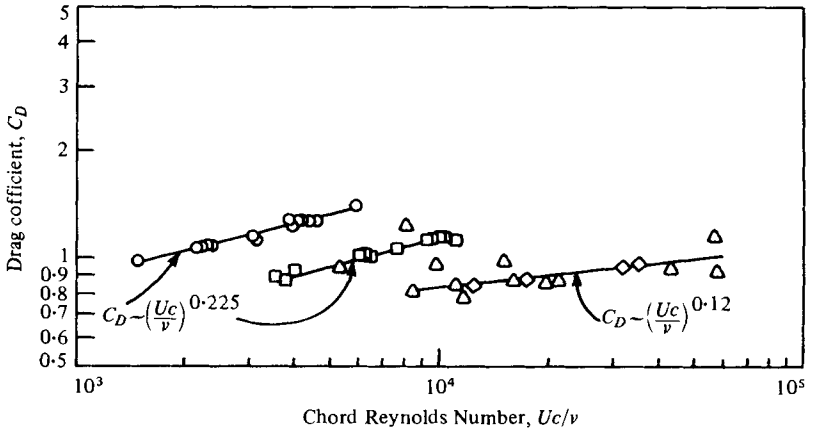

FIGURE 19. Drag coefficient *vs.* chord Reynolds number with thickness Reynolds number as a parameter. Free-flight data from Dupleich. Ut/ν: ○, 38–47; □, 91–104; △, 119–1930; ◇, 693–725.

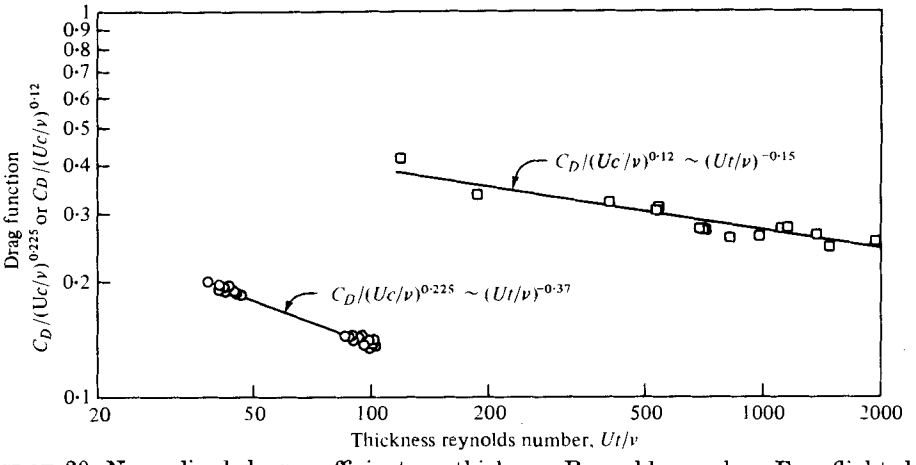

FIGURE 20. Normalized drag coefficient *vs.* thickness Reynolds number. Free-flight data from Dupleich, Uc/ν: ○, 1470–11250; □, 5280–57750.

The drag coefficient is plotted *vs.* a combined Reynolds number function in figure 21. For thickness Reynolds numbers $38 \leqslant Ut/\nu \leqslant 104$,

$$C_D \simeq 0{\cdot}78(Uc/\nu)^{0·225}(Ut/\nu)^{-0·37} = 0{\cdot}77 f_5(Uc/\nu, Ut/\nu), \tag{23a}$$

and for thickness Reynolds numbers $119 \leqslant Ut/\nu \leqslant 1930$,

$$C_D \simeq 0{\cdot}77(Uc/\nu)^{0·12}(Ut/\nu)^{-0·15} = 0{\cdot}77 f_5(Uc/\nu, Ut/\nu). \tag{23b}$$

Free-flight data from Bustamante & Stone (1969) for an autorotor of aspect ratio 1·19 are also plotted in figure 21 according to (23*b*). Their Reynolds numbers are about 20 times the largest values from Dupleich's data, thus (23*b*) is not likely to be applicable. As a result, the two data points lie somewhat above the curve which fits Dupleich's data. The lift–drag ratio from Dupleich's results is illustrated in figure 22, plotted *vs.* the ratio of the right sides of (22) and (23). Again the agreement is good.

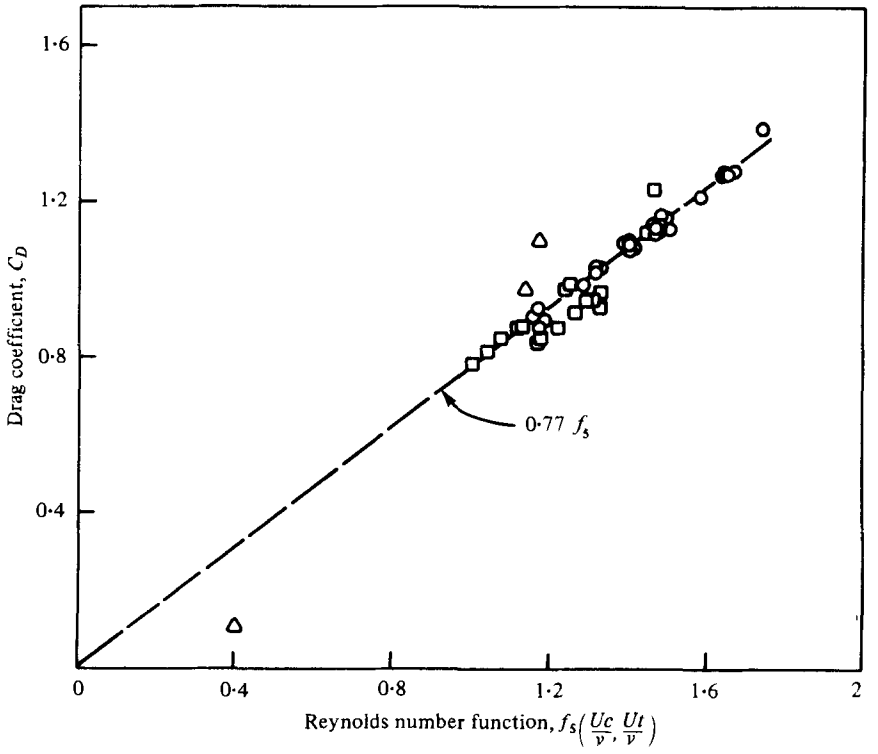

FIGURE 21. Drag coefficient *vs.* Reynolds number function. Free-flight data.

		Uc/ν	Ut/ν	F
Dupleich	○	1470–11250	38–104	$1{\cdot}01(Uc/\nu)^{0{\cdot}225}/(Ut/\nu)^{0{\cdot}37}$
	□	5280–57750	119–1930	$(Uc/\nu)^{0{\cdot}12}/(Ut/\nu)^{0{\cdot}15}$
Bustamente & Stone	△	$1{\cdot}1 \times 10^6$	$2{\cdot}8 \times 10^4$	$(Uc/\nu)^{0{\cdot}12}/(Ut/\nu)^{0{\cdot}15}$

8. Conclusions

To the author's knowledge, there have been only two comprehensive systematic series of experiments concerning the autorotation of flat-plate wings: that in free flight by Dupleich (1941) and that in a wind tunnel by Glaser & Northup (1971). The wind-tunnel experiments of Smith (1970, 1971), while carried out very carefully and with a minimum amount of bearing friction, were concerned primarily with wings with various types of tip plates instead of a consistent family of shapes such as flat-plate wings of varying thickness and aspect ratio. In Dupleich's case, correlation of the data was done only in terms of dimensional quantities, which makes interpretation of his figures very difficult. Northup & Glaser did present their results in a systematic fashion in terms of moment-of-inertia and thickness parameters but did not make a thorough comparison of their results with Dupleich's free-flight data. Smith's interpretation of the wind-tunnel results in terms of Strouhal number *vs.* Reynolds number has been shown in this paper to be incorrect and to predict values of the tip-speed ratio V/U which are too small. The fact that the tip-speed ratio is relatively independent of the Reynolds number, contrary to Smith's conclusions, is shown by figure 14, where the

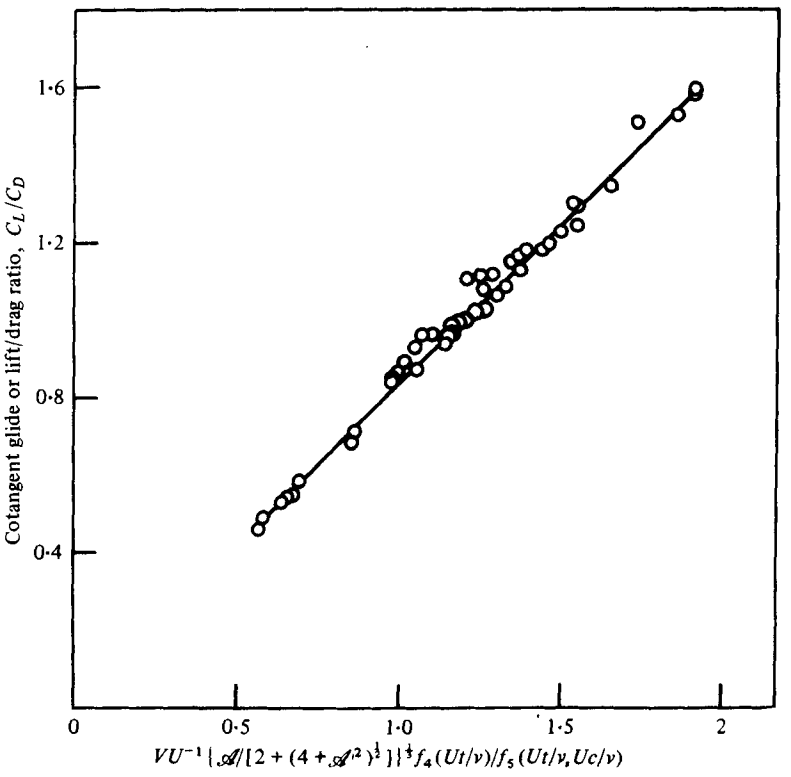

FIGURE 22. Lift–drag ratio *vs.* tip-speed ratio–aspect ratio–Reynolds number function. Free-flight data from Dupleich, $0{\cdot}8 \leqslant \mathscr{A} \leqslant 6$, $0{\cdot}0074 \leqslant \tau \leqslant 0{\cdot}167$, $38 \leqslant Ut/\nu \leqslant 1930$, $1470 \leqslant Uc/\nu \leqslant 57750$. For $f_4(Ut/\nu)$, see figure 16. For $f_5(Ut/\nu, Uc/\nu)$, see equation (23).

free-flight data of Bustamante & Stone compare well with wind-tunnel data and Dupleich's free-flight data for much smaller Reynolds numbers.

Tip-speed ratio data from both a wind tunnel and free flight have been shown to correlate well and in the same fashion with the aspect ratio and thickness ratio (figures 6–9). It was shown that, because of bearing friction, the appropriate tip-speed ratio is found from the slope of the tip-speed curve. For a given wing geometry, it was shown that a minimum moment-of-inertia parameter exists below which autorotation is impossible. For values of the moment-of-inertia parameter greater than one, the tip-speed ratio is nearly independent of the moment of inertia. The minimum inertial parameter is less in free flight than in a wind tunnel because of bearing friction. The variation of the tip-speed ratio for very small values of the moment of inertia is also different in free flight. The reason for this is unknown but may be because variation in aerodynamic effects with changes in cyclic pattern is masked in a wind tunnel by effects of bearing friction.

The lift coefficient of autorotating plates was shown to be a function of the aspect ratio, tip-speed ratio and the Reynolds number based on the plate thickness, while the drag coefficient, which is independent of the aspect ratio, is a function of two Reynolds numbers, one based on the thickness and one on the chord. For higher Reynolds numbers, the variation with Reynolds number becomes weaker. This trend would be expected to continue for Reynolds numbers higher than the range investigated.

For practical purposes, it would be advantageous to be able to predict the flight-path glide angle and speed for a given autorotating wing. If the wing were not too light, the glide angle, tip-speed ratio and other dimensionless parameters would be independent of the moment-of-inertia parameter. The glide angle would, however, still be a complicated function of the aspect ratio, thickness ratio and thickness and chord Reynolds numbers. Within the ranges of the parameters covered, the glide angle can be predicted from the figures in this paper.

REFERENCES

ACKERET, J. 1925 Neure Untersuchungen der Aerodynamischen Versuchsanstalt, Göttingen. *Z. Flugtech. Motorluftschiffahrt* **16**, 44.

AHLBORN, F. 1930 The Magnus effect in theory and reality. *N.A.C.A. Tech. Memo* no. 567.

ALVAREZ-CALDERON, A. & ARNOLD, F. R. 1961 A study of the aerodynamic characteristics of a high-lift device based on a rotating cylinder and flap. *Stanford Univ. Tech. Rep. RCF-1.*

BLACKWELL, B. F. 1974 The vertical axis wind turbine 'how it works.' *Sandia Lab., Albuquerque, New Mexico Rep.* SAND 74-0435.

BRUNK, J. E. 1965 Application of a semi-rectangular autorotating cylinder to a high-lift wing and flap combination. *Alpha Res. Inc. Rep.* no. 65-1.

BUFORD, W. E. 1954 Magnus effect in the case of rotating cylinders and shall. *Ballistic Res. Lab. Aberdeen Proving Ground, Md. Memo Rep.* no. 821.

BUSTAMANTE, A. G. & STONE, G. W. 1969 The autorotation characteristics of various shapes for subsonic and hypersonic flows. *A.I.A.A. Paper* no. 69-132.

CRABTREE, L. F. 1960 The rotating flap as a high-lift device. *Aero. Res. Counc. Current Paper* no. 480.

DIEDERICH, F. W. 1951 A planform parameter for correlating certain characteristics of swept wings. *N.A.C.A. Tech. Note* no. 2335.

DUPLEICH, P. 1941 Rotation in free fall of rectangular wings of elongated shape. *N.A.C.A. Tech. Memo* no. 1201.

GLASER, J. C. & NORTHUP, L. L. 1971 Aerodynamic study of autorotating flat plates. *Engng Res. Inst., Iowa State Univ. Ames, Rep.* ISU-ERI-Ames 71037.

IVERSEN, J. D. 1969 The Magnus rotor as an aerodynamic decelerator. *Proc. Aerodyn. Deceleration Systems Conf.* vol. 2, pp. 385–395. Air Force Flight Test Center, Edwards AFB, California.

IVERSEN, J. D. 1973 Correlation of Magnus force data for slender spinning cylinders. *J. Spacecraft Rockets* **10**, 268–272.

JACOBSON, I. D. 1973 Magnus characteristics of arbitrary rotating bodies. *Agardograph* no. 171.

KELLY, H. R. 1954 An analytical method for predicting the Magnus forces and moments on spinning projectiles. *U.S. Naval Ord. Test Stn, China Lake, Calif., Tech. Memo* no. 1634.

KELLY, H. R. & THACKER, G. R. 1956 The effect of high spin on the Magnus force on a cylinder at small angles of attack. *NAVORD Rep.* no. 5036.

KLEMIN, A. 1925 The Savenius wing rotor. *Mech. Engng* **47**, 911.

KLEMIN, A. 1932 A rotor airplane. *Sci. Am.* **146**, 362.

MAGNUS, G. 1853 Ueber die Abseichung der Geschosse. *Poggendorfer Ann. Phys.* **88**, 604.

MAXWELL, J. C. 1854 Rotation of a falling card. *Camb. Dublin Math. J.* **9**, 145.

PLATOU, A. S. 1961 The Magnus force on a rotating cylinder in transonic cross flows. *Ballistic Res. Lab. Aberdeen Proving Ground, Md, Rep.* no. 1150.

POWER, H. L. & IVERSEN, J. D. 1973 Magnus effect on spinning bodies of revolution. *A.I.A.A. J.* **11**, 417–418.

REGAN, F. J. 1966 Magnus effects. *The Fluid Dynamic Aspects of Ballistics. Agard Conf. Proc.* no. 10.

REID, E. G. 1924 Tests of rotating cylinders. *N.A.C.A. Tech. Note* no. 209.

RIABOUCHINSKY, D. P. 1935 Thirty years of theoretical and experimental research in fluid mechanics. *J. Roy. Aero. Soc.* **35**, 282–348, 377–444.

SAVONIUS, S. J. 1926 *The Wing-Rotor in Theory and Practice*. Helsingfors, Finland: Savonius.

SMITH, E. H. 1970 Autorotating wings: an experimental investigation. *Univ. Michigan Aerospace Engng Rep.* no. 01954-2-7.

SMITH, E. H. 1971 Autorotating wings: an experimental investigation. *J. Fluid Mech.* **50**, 513–534.

SWANSON, W. M. 1961 The Magnus effect: a summary of investigations to date. *J. Basic Engng* **82**, 461–470.

THOM, A. 1934 On the effect of discs on the air forces on a rotating cylinder. *Aero. Res. Counc. R. & M.* no. 1623.

USELTON, J. C. 1966 Investigation of the Magnus effects and the effects of unsymmetrical leeward vortex patterns of a high fineness ratio model at Mach numbers 3 and 5. M.Sc. thesis, University of Tennessee. (See also *AEDC Tech. Rep.* no. 66–171.)

VORREITER, J. W. & TATE, D. L. 1973 Observations of disk-shaped bodies in free flight at terminal velocity. *N.A.S.A. Tech. Memo* no. X-62262.

WILLHOFT, R. O. 1927 Industrial applications of the Flettner rotor. *Mech. Engng.* **49**, 249.

WOLFF, E. B. & KONIG, C. 1926 Tests for determining the effect of a rotating cylinder fitted into the leading edge of an airplane wing. *N.A.C.A. Tech. Memo* no. 354.

YELMGREN, K. 1966 The autorotation of Magnus rotors. *Dept. Aerospace Engng, Univ. Notre Dame, Indiana, Rep.*